

Electronic Supplementary Information

Reversible reconstructive transition of $[\text{CuZn}(\text{CN})_4]^-$ framework host induced by guest exchange

S. Nishikiori

Department of Basic Science, Graduate School of Arts and Sciences, The University of Tokyo

3-8-1 Komaba, Meguro, Tokyo 153-8902, Japan

Phone & FAX : +81 3 5454 6569

Email : cnskor@mail.ecc.u-tokyo.ac.jp

Preparation of $[(\text{CH}_3)_3\text{NH}][\text{CuZn}(\text{CN})_4] \cdot n\text{H}_2\text{O}$ ($n = 1.5$).

After $\text{K}_2[\text{Zn}(\text{CN})_4]$ (3.5 mmol, 0.87 g) and KCN (9.0 mmol, 0.59 g) were dissolved in 20 mL of water, CuCN (5.25 mmol, 0.47 g) and $(\text{CH}_3)_3\text{N}\cdot\text{HCl}$ (1.75 mmol, 0.17 g) were added. The solution was slightly boiled for 60 m with stirring, and then cooled down to room temperature. The target compound was filtered as white powder. (Found: C, 26.15; H, 4.30; N, 21.54; Cu+Zn, 40.4. Calc. for $\text{C}_7\text{H}_{13}\text{N}_5\text{O}_{1.5}\text{CuZn}$: C, 26.26; H, 4.09; N, 21.87; Cu+Zn, 40.3%) The quantitative determination of Cu+Zn was carried out by chelate titration after the Cu/Zn ratio was confirmed to be 1 by ICP analysis.

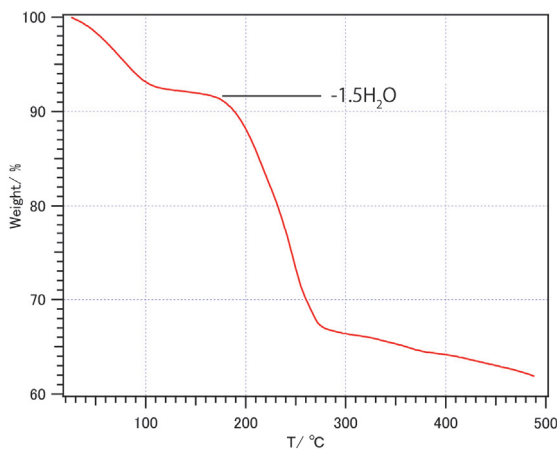


Fig. ESI-1. TG curve for the powder of $[(\text{CH}_3)_3\text{NH}][\text{CuZn}(\text{CN})_4] \cdot n\text{H}_2\text{O}$ ($n = 1.5$). The first decrease observed between 30 and ca. 150 °C corresponds to the liberation of $1.5\text{H}_2\text{O}$.

Thermogravimetric analysis (TG) was carried out using TA instruments TGA 2950 thermobalance at 20 K/min scan rate under N_2 gas flow. IR spectra were measured by the attenuated total reflection (ATR) method using JASCO FT/IR-4100 spectrometer. Note that due to a diamond anvil (JASCO ATR PRO450-S) used in the ATR method some distortion of the base line is seen between 2500 and 1800 cm^{-1} . Powder X-ray diffraction patterns were measured using Bruker D8Advance diffractometer equipped with LynxEye 1-dimensional detector. The measurements were carried out using $\text{Cu K}\alpha$ radiation ($\lambda = 1.5418 \text{ \AA}$) in a scan range between $2\theta = 5^\circ$ and 60° with a step width of 0.0235° and interval time of 0.2 s/step at room temperature. Measurements of solid-state ^{13}C and ^2H NMR spectra were carried out using Bruker Avance 400 spectrometer. Larmor frequencies for ^{13}C and ^2H were 100.63 and 61.43 MHz, respectively. For ^{13}C NMR spectra, a simple pulse sequence which is formed with a 90° pulse with 4.5 μs pulse width and successive high power decoupling for ^1H was used. Cross polarization technique was ineffective because of fast isotropic motion of the guest. MAS (magic angle spinning) rate was 5000 Hz. In the measurement of ^2H -NMR powder patterns, quadrupole echo pulse sequence with a 90° pulse with 2.5 μs pulse width, 30 μs spacing time and 5 s repetition time was used.

sample	(a)		(b)		(e)		(f)	
<i>h k l</i>	2θ(obs)/°	2θ(calc)/°	2θ(obs)/°	2θ(calc)/°	2θ(obs)/°	2θ(calc)/°	2θ(obs)/°	2θ(calc)/°
1 1 1	13.18	13.18	13.19	13.19	13.19	13.18	13.33	13.33
2 0 0	15.23	15.23	15.27	15.24	15.23	15.23	15.41	15.40
2 1 0							17.24	17.24
2 1 1							18.90	18.90
2 2 0	21.61	21.61	21.67	21.62	21.61	21.61	21.85	21.85
3 0 0							23.20	23.20
3 1 0							24.47	24.47
3 1 1	25.39	25.40	25.45	25.41	25.39	25.40	25.68	25.68
2 2 2	26.54	26.55	26.60	26.56	26.55	26.55	26.85	26.85
3 2 0							27.97	27.96
3 2 1							29.04	29.04
4 0 0	30.73	30.75	30.81	30.76	30.74	30.75	31.11	31.10
4 1 0							32.08	32.08
3 3 1	33.58	33.58	33.63	33.60	33.58	33.58	33.96	33.97
4 2 1							35.77	35.77
3 3 2							36.65	36.64
4 2 2	37.90	37.89	37.93	37.91	37.89	37.89	38.33	38.33
5 0 0							39.15	39.15
5 1 0							39.96	39.96
5 1 1	40.28	40.29	40.32	40.30	40.32	40.29	40.74	40.76
5 2 0							42.33	42.31
5 2 1							43.09	43.07
4 4 0	44.04	44.04	44.07	44.06	44.04	44.04	44.56	44.55
4 4 1							45.26	45.28
5 3 0							46.00	46.00
5 3 1	46.17	46.17	46.20	46.19	46.16	46.17	46.71	46.71
6 2 0	49.57	49.56	49.59	49.59	49.59	49.56	50.15	50.15
5 4 0							50.80	50.82
5 4 1							51.49	51.48
5 3 3	51.50	51.52	51.53	51.54	51.55	51.52	52.11	52.14
cell param.	cubic $a = 11.6228(7)$ Å		cubic $a = 11.618(2)$ Å		cubic $a = 11.623(1)$ Å		cubic $a = 11.4949(5)$ Å	

sample	(c)		(d)	
<i>h k l</i>	2θ(obs)/°	2θ(calc)/°	2θ(obs)/°	2θ(calc)/°
1 0 0	12.38	12.37	12.34	12.34
0 0 2	13.15	13.16	13.24	13.23
1 0 1	14.04	14.02	14.01	14.01
1 0 2	18.10	18.10	18.14	18.13
1 1 0	21.52	21.51	21.45	21.45
1 0 3	23.39	23.41	23.50	23.49
1 1 2	25.30	25.30	25.30	25.29
2 0 1	25.77	25.76	25.72	25.71
0 0 4	26.50	26.50	26.67	26.65
2 0 2	28.30	28.25	28.23	28.23
1 0 4	29.31	29.34	29.47	29.46
2 0 3	31.99	32.00	32.02	32.02
2 1 0	33.15	33.12	33.04	33.03
2 1 1	33.80	33.80	33.73	33.72
1 0 5	35.67	35.64	35.81	35.81
3 0 0	37.73	37.71	37.62	37.61
2 1 3	38.89	38.88	38.87	38.87
0 0 6	40.17	40.21		
2 0 5	42.03	42.01	42.13	42.13
2 2 0	43.84	43.82	43.70	43.71
2 2 2	45.92	45.95	45.86	45.87
1 1 6			46.23	46.23
2 1 5	47.75	47.77	47.74	47.75
3 1 3	50.26	50.27	50.21	50.20
cell param.	hexagonal $a = 8.255(1)$ Å $c = 13.447(3)$ Å		hexagonal $a = 8.2778(4)$ Å $c = 13.370(1)$ Å	

Table ESI-1. List of powder X-ray diffraction peaks in Fig. 2 and their assignment.

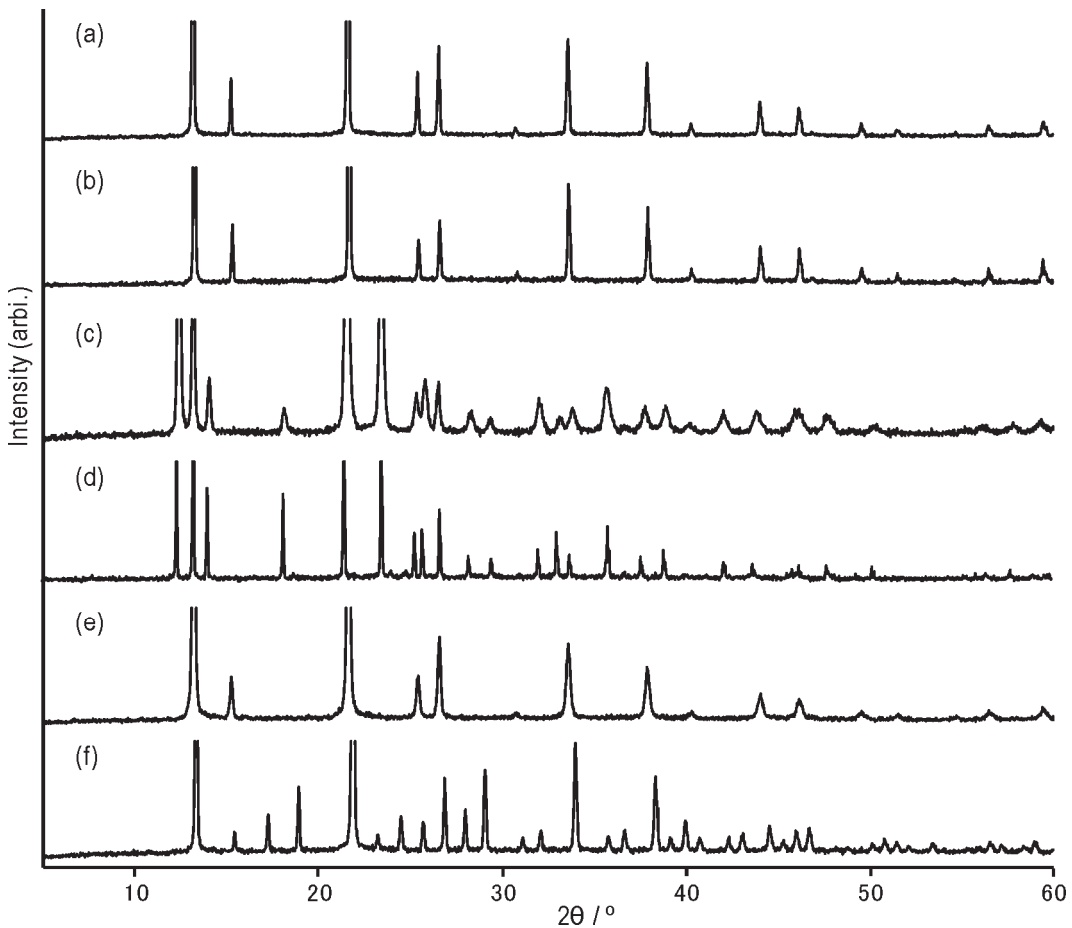


Fig. ESI-2. Powder X-ray diffraction patterns. Enlarged view of Fig. 2.

All diffraction peaks in Fig. 2 of the main text and their assignment are listed in Table ESI-1: (a) $[(\text{CH}_3)_3\text{NH}][\text{CuZn}(\text{CN})_4] \cdot 1.5\text{H}_2\text{O}$ as prepared (CRI form); (b) $[(\text{CH}_3)_4\text{N}][\text{CuZn}(\text{CN})_4]$. Its cell parameters previously reported are $a = 11.671(2)$ Å with space group $F\bar{4}3m$ [3]; (c) $[(\text{CH}_3)_3\text{NH}][\text{CuZn}(\text{CN})_4] \cdot \text{CH}_3\text{CN}$ which is (a) exposed to acetonitrile vapour at 30°C for 5 d. (TRI form); (d) $[\text{K}(\text{H}_2\text{O})_n][\text{CuZn}(\text{CN})_4](n=7.5)$. The cell parameters previously reported for $[\text{K}(\text{H}_2\text{O})_n][\text{CuZn}(\text{CN})_4]$ ($n=11.2$) are $a = 8.2737(8)$ Å and $c = 13.4002(13)$ Å with space group $P6_3mc$.[1]; (e) (c) exposed to water vapour at 30°C for 1 d. (CRI form); (f) (a) exposed to acetonitrile vapour at 30°C for 30 m. $2\theta(\text{obs})$ and $2\theta(\text{calc.})$ in Table ESI-1 are the angles of diffraction peaks observed and derived from indexing calculations by TREOR90[2], respectively. In the bottom of the list, cell parameters that TREOR90 calculated are shown. The resultant assignments of (a), (b) and (e) well agree with each other. That of (f) also well agrees with those of (a), (b) and (e). However, in (f) peaks which are originally absent due to the extinction rule of all-face centered cubic cell($F\bar{4}3m$) were observed and cell parameters for (f) are slightly smaller than those of the three samples. The agreement between TRI form samples, (c) and (d), is also good.

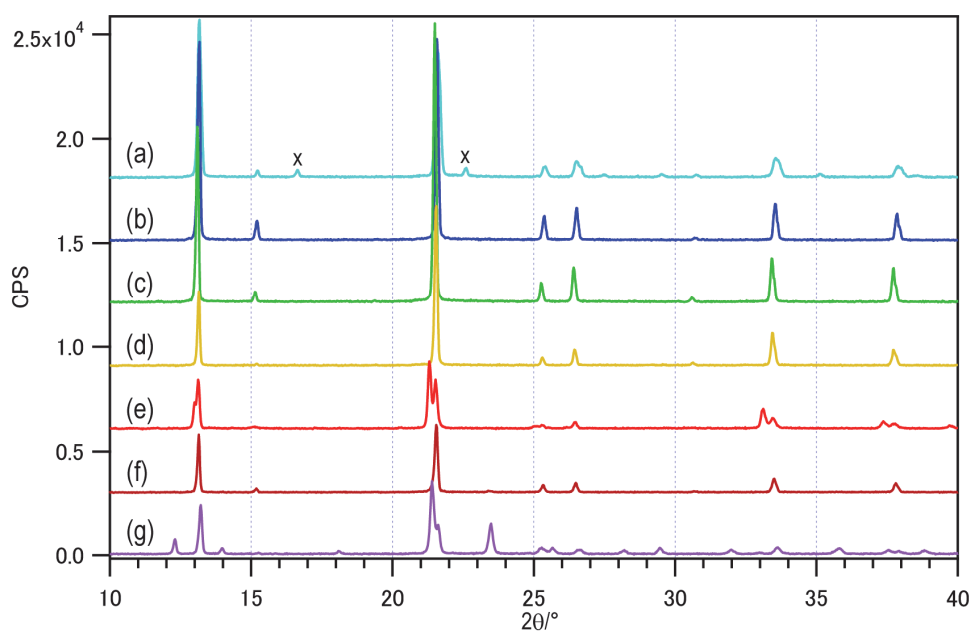
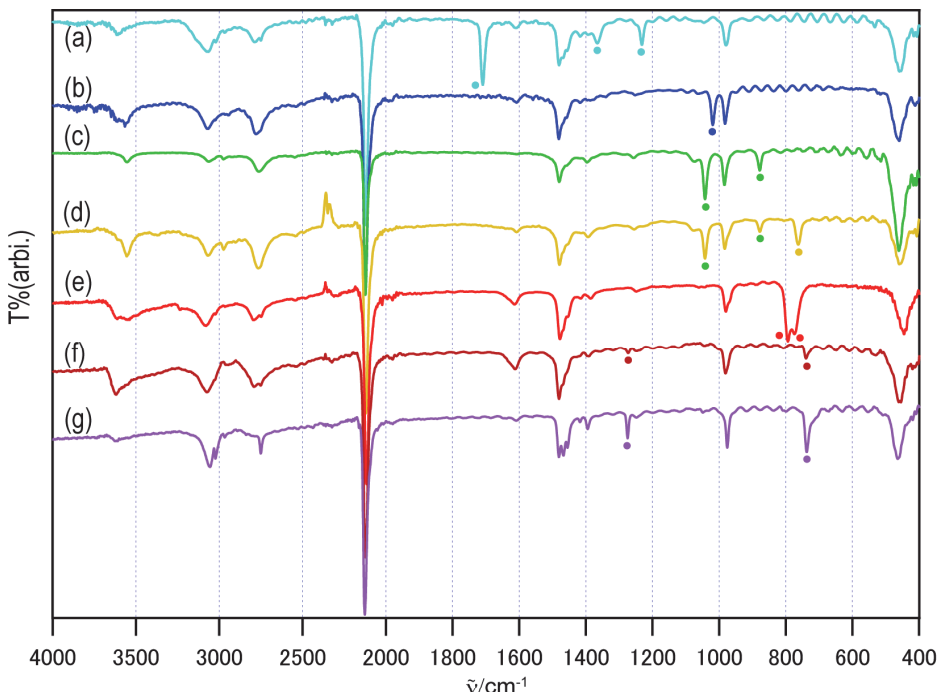


Fig. ESI-3. IR spectra (up) and powder X-ray diffraction patterns (bottom) of $[(\text{CH}_3)_3\text{NH}][\text{CuZn}(\text{CN})_4] \cdot 1.5\text{H}_2\text{O}$ after exposure to various vapours at room temperature for 100 d. (a) acetone; (b) methanol; (c) ethanol; (d) CHCl_3 ; (e) CCl_4 ; (f) CH_2Cl_2 (exposed for 21 d); (g) CH_2Cl_2 . Note that IR spectra were measured by ATR method using a diamond anvil so that some distortion of the base line is seen around 2300 cm^{-1} especially in (d) and (e).

In Fig. ESI-3, characteristic IR signals of each compound in the fingerprint region are marked with ●. Except in the cases of (c) and (g), signals of water remained so that replacement of water is uncompleted. Interestingly, in the case of (d) CHCl_3 signals of ethanol were observed. Its origin is considered to be stabilizing additive originally added to commercially produced CHCl_3 . Solid-state ^{13}C NMR spectrum also showed signals of ethanol. This host is likely to have very strong affinity to ethanol. In the powder X-ray diffraction pattern of (a) acetone, two additional peaks marked with x were

observed. There may be some distortion or degradation of CRI lattice. In the case of CH_2Cl_2 , two PXRD patterns of CRI (f) and TRI (g) were observed corresponding to the difference in the exposure time, though the TRI pattern of (g) is not clear as the case of acetonitrile (Fig. 2(c) and ESI-2(c)). In other measurements for CH_2Cl_2 , in some cases CRI form pattern was observed but in other cases TRI form pattern appeared. CH_2Cl_2 can induce the structural change from CRI to TRI form. However, its reproducibility is poor.

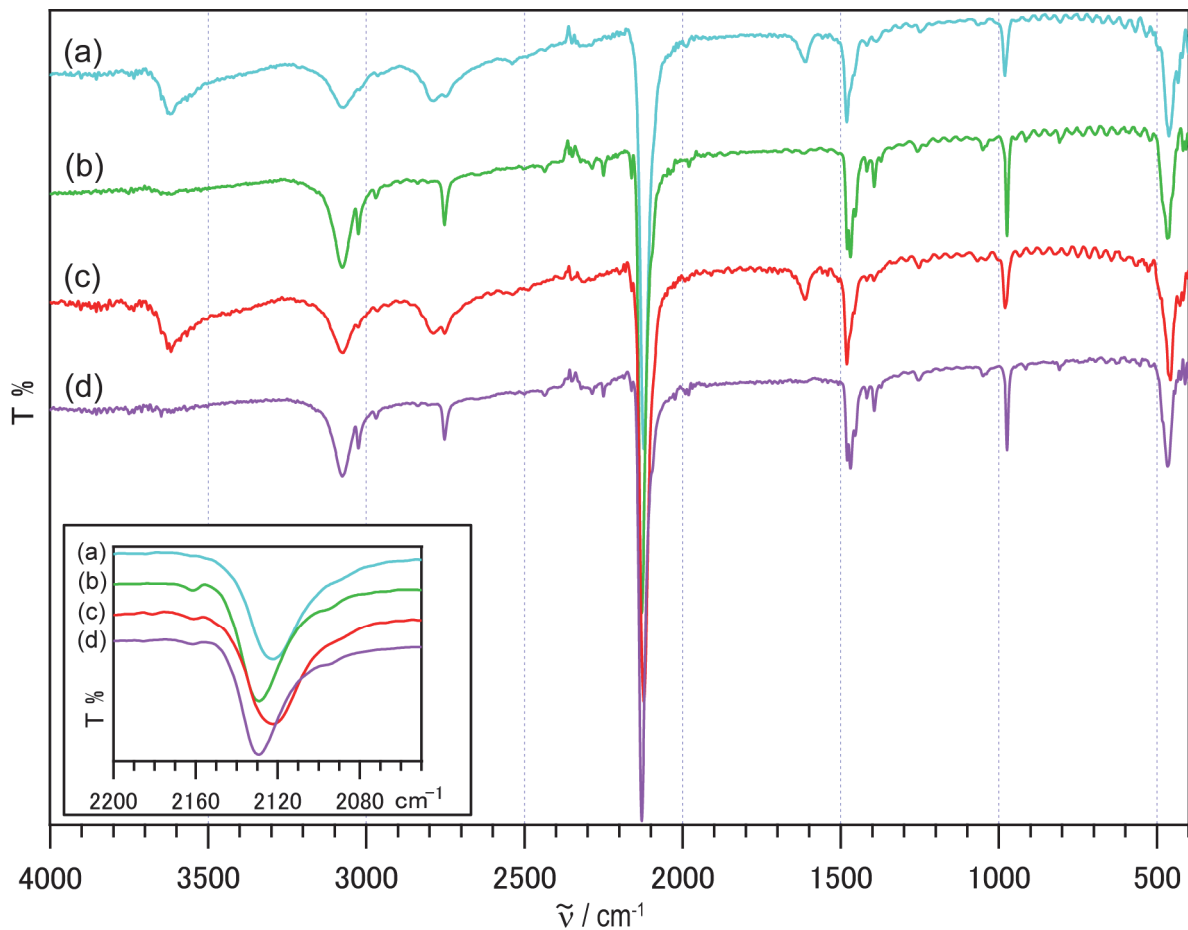


Fig. ESI-4. IR spectra along the process in which water and acetonitrile were exchanged alternately. (a) $[(\text{CH}_3)_3\text{NH}][\text{CuZn}(\text{CN})_4]\cdot 1.5\text{H}_2\text{O}$ as prepared. (CRI form); (b) (a) exposed to acetonitrile vapour at 30°C for 5 d. (TRI form); (c) (b) exposed to water vapour at 30°C for 1 d. (CRI form); (d) (c) exposed to acetonitrile vapour at 30°C for 5 d. (CRI form). The inset is enlarged view of $\text{C}\equiv\text{N}^-$ stretch band of $[\text{CuZn}(\text{CN})_4]^-$ framework. In TRI form no splitting but shift to higher wavenumber region was observed.

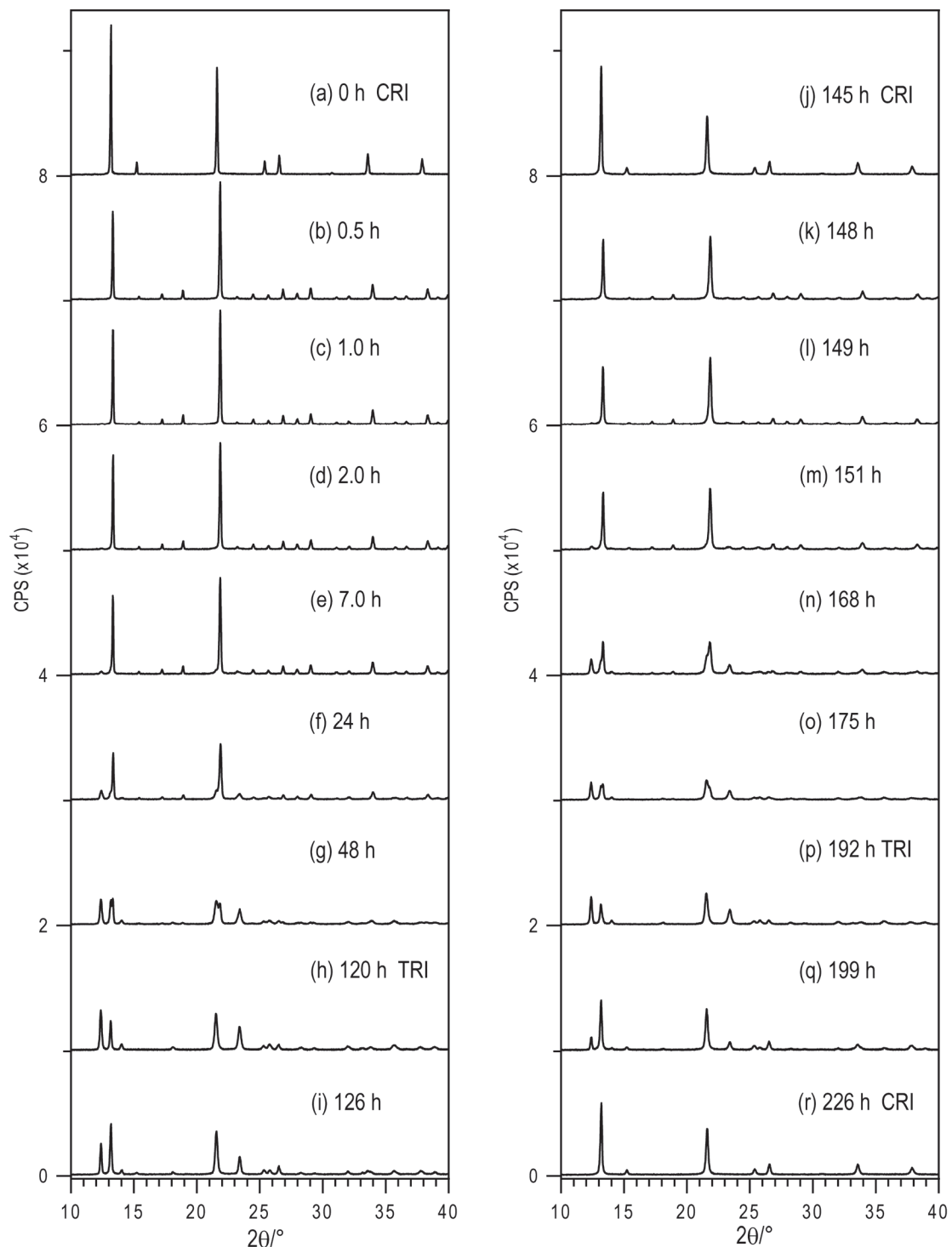


Fig. ESI-5. Powder X-ray diffraction patterns along the process in which water and acetonitrile were exchanged alternately. The time indicated is elapsed time in hour. (a) $[(CH_3)_3NH][CuZn(CN)_4] \cdot 1.5H_2O$ as prepared. (CRI form); (b)-(h) patterns of the sample exposed to acetonitrile vapour at $30^\circ C$. (i)-(j) those exposed to water vapour at $30^\circ C$; (k)-(p) those exposed to acetonitrile vapour at $30^\circ C$; (q)-(r) those exposed to water vapour at $30^\circ C$. Pattern change over two cycles is presented here. These changes were observed over more than 10 cycles.

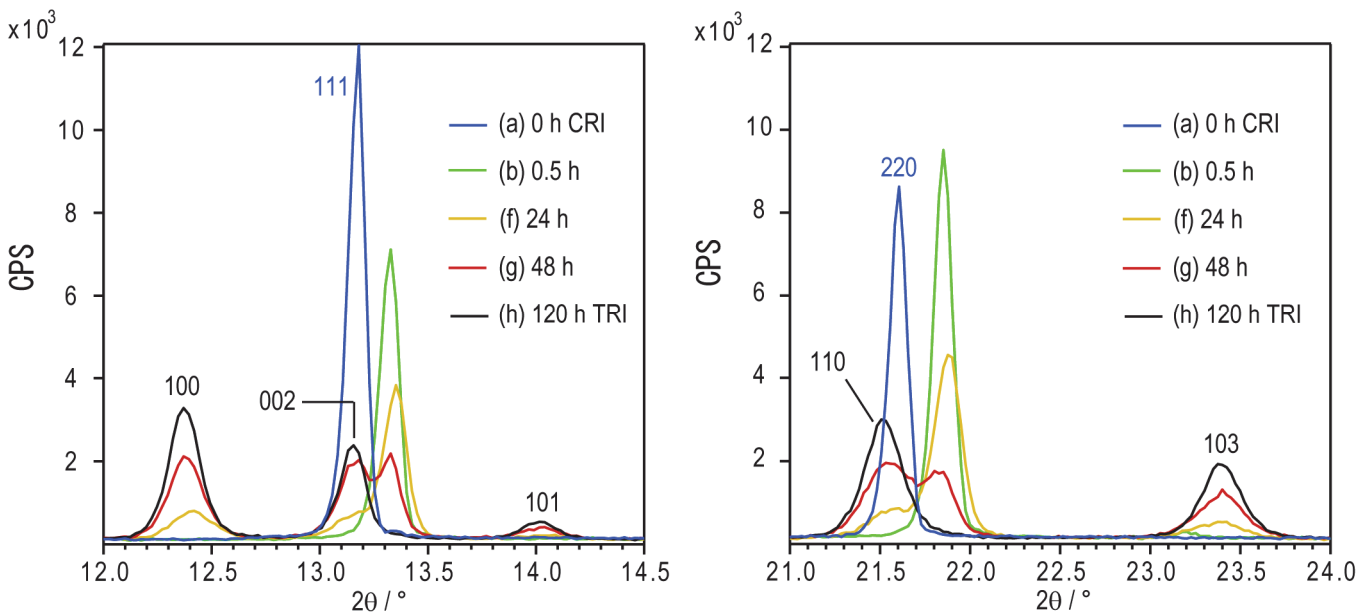


Fig. ESI-6. Powder X-ray diffraction patterns around diffraction peaks of 111 and 220 during the transition from CRI to TRI form. The legend is same as that of Fig. ESI-5. When the sample was placed in acetonitrile vapour, the peaks shifted to higher angle region, namely the crystal lattice shrunk. This shrink occurred within a few minutes. The cell parameters for the shrunk lattice are shown in Table ESI-1(f). Then the peaks assigned as 111 and 220 in CRI form were gradually recovered at their almost original positions. They are considered to become the peaks of 002 and 110 in TRI form, respectively.

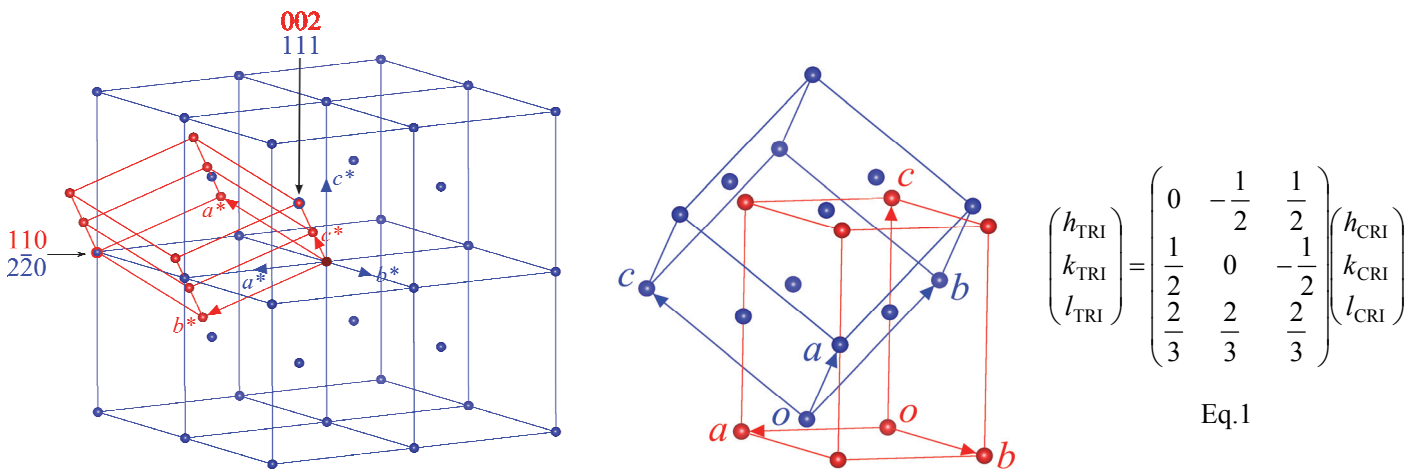


Fig. ESI-7. Relationship between CRI form lattice (blue) and TRI form lattice (red) in the reciprocal space (left) and the direct space (center) on the assumption that the diffractions of $\bar{2}\bar{2}0$, $2\bar{0}\bar{2}$ and 111 in CRI form become those of 110, $\bar{1}20$ and 002 in TRI form, respectively. Eq.1 is the transformation matrix between the two lattices.

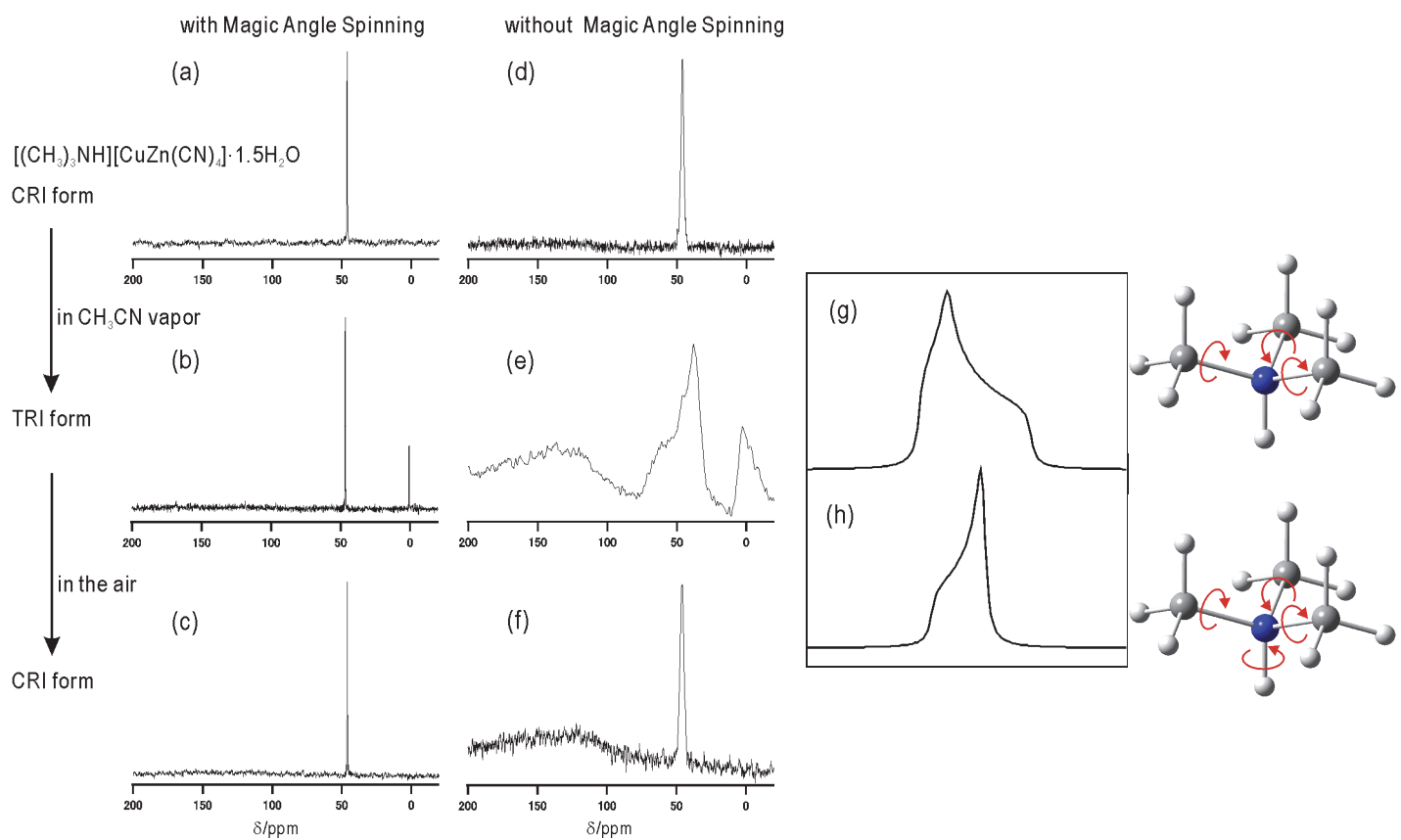


Fig. ESI-8. Solid-state ^{13}C NMR spectra of CRI and TRI form samples ((a)-(f)) and line shapes simulated for C in a methyl group ((g),(h)).

Fig. ESI-8(a), (d) and (b), (e) are spectra observed before and after placing the sample in acetonitrile vapour, respectively. After the measurement of (b), and (e), the sample was placed in the air. Then (c) and (f) were observed. (a), (b) and (c) were measured as high resolution spectra using MAS to confirm the guest species. (d), (e) and (f) were measured under stationary condition to observe the chemical shift shielding tensor averaged by guest molecular motion. The signal at 46.1 ppm comes from C of $(\text{CH}_3)_3\text{NH}^+$. Very sharp line shapes in (d) and (f) show fast isotropic reorientational motion of $(\text{CH}_3)_3\text{NH}^+$. On the other hand, in (e), where acetonitrile is included instead of H_2O , so-called axial powder pattern was observed. This line shape suggests that $(\text{CH}_3)_3\text{NH}^+$ undergoes rotational motion about its C_3 axis. (g) is the line shape simulated on the assumption that the orientation of the whole $(\text{CH}_3)_3\text{NH}^+$ ion is fixed but each methyl group undergoes rotational motion about each C_3 axis of the methyl group. Moreover, (h) is the spectrum expected for the case that $(\text{CH}_3)_3\text{NH}^+$ undergoes rotational motion about the C_3 axis of the ion and, needless to say, the rotational motion of each methyl group remains. The agreement between (e) and (h) is well so that the orientation of $(\text{CH}_3)_3\text{NH}^+$ which is free in CRI form is fixed in TRI form. There is no space around $(\text{CH}_3)_3\text{NH}^+$ in TRI form. The signals observed at *ca.* 0 ppm in (b) and (e) come from the methyl carbon of the trapped acetonitrile. In (e) the signal was observed as a powder pattern. This suggests the orientation of the acetonitrile might be fixed. For this point clearer information was obtained from ^2H -NMR powder pattern (Fig. ESI-10). The broad signals observed over the range between *ca.* 100 and 200 ppm in (d), (e) and (f) come from the carbon in the

probe of the NMR spectrometer and in the cap of the sample holder because the measurements were carried out under high sensitive conditions without cross polarization.

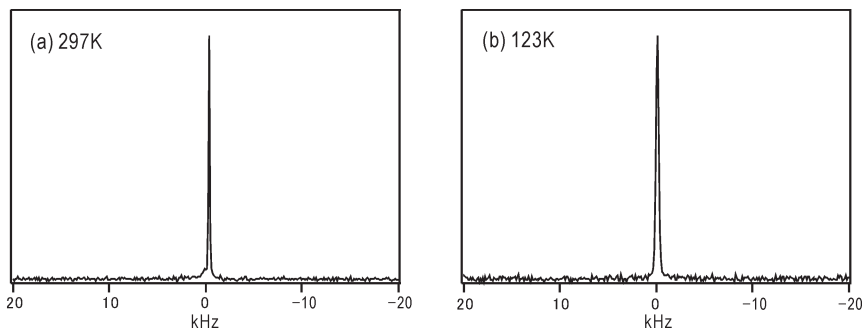


Fig. ESI-9. ^2H -NMR powder patterns of CRI form $[(\text{CH}_3)_3\text{NH}][\text{CuZn}(\text{CN})_4]$ including D_2O instead of H_2O .

The sample was prepared by standing powder of $[(\text{CH}_3)_3\text{NH}][\text{CuZn}(\text{CN})_4] \cdot 1.5\text{H}_2\text{O}$ in D_2O vapour. The very shape line observed indicates fast isotopic reorientaional motion of D_2O . Almost same line shape was observed at 123 K so that the activation energy for the isotopic motion is considerably low, namely there is sufficient free space around the D_2O molecule. Considering that the D_2O molecule is trapped in the cavity of CRI form lattice with T_d symmetry, these results are reasonable.

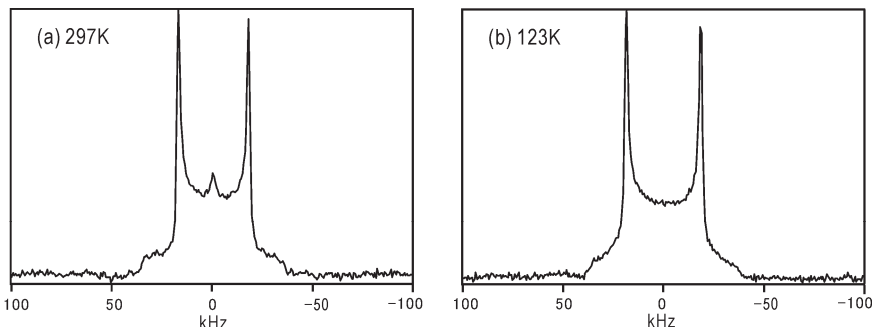


Fig. ESI-10. ^2H -NMR powder patterns of TRI form $[(\text{CH}_3)_3\text{NH}][\text{CuZn}(\text{CN})_4]$ including CD_3CN .

The sample was prepared by standing powder of $[(\text{CH}_3)_3\text{NH}][\text{CuZn}(\text{CN})_4] \cdot 1.5\text{H}_2\text{O}$ in CD_3CN vapour. The axial powder pattern observed at 297 K is a typical pattern that appears for a deuterated methyl group rotating about its own C_3 axis. At the same time, this pattern indicates that the orientation of the CD_3CN molecule is fixed. The powder pattern at 123 K is essentially identical to that at 297 K. This strongly suggests that there is no space around the CD_3CN molecule. If there is room around the guest molecule, the guest molecular motion usually becomes more vigorous and the powder pattern changes its shape and width with increasing temperature.

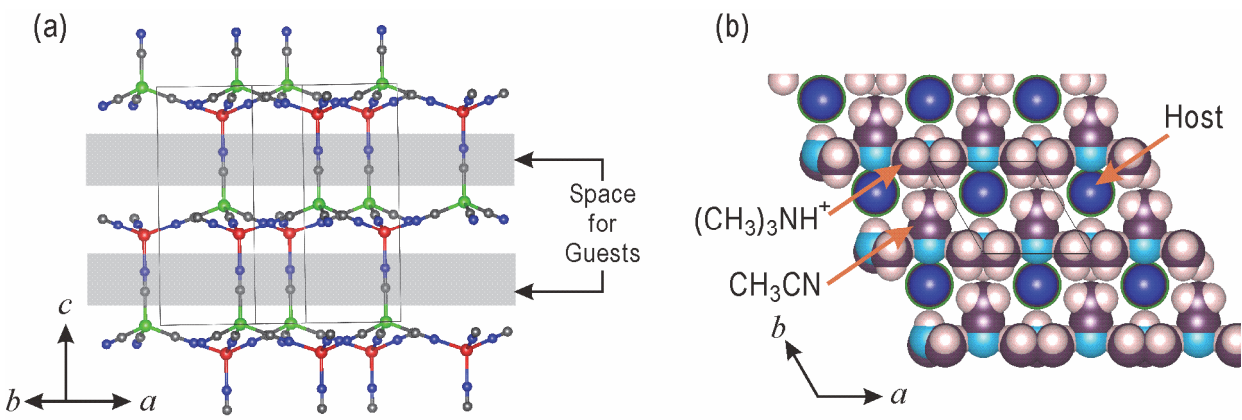


Fig. ESI-11. (a) Probable space for accommodating the guests, $(\text{CH}_3)_3\text{NH}^+$ and CH_3CN , in TRI form host. The space spreads two dimensionally parallel to the ab plane of TRI form crystal. (b) A possible packing of guest molecules in the two dimensional space. All atoms are illustrated with their van der Waals radii. Although there are pillars of CN^- bridges here and there, close packing of $(\text{CH}_3)_3\text{NH}^+$ and CH_3CN is possible. However, many possibilities for such arrangement of the guests including disordered cases can be considered. It is difficult to know actual arrangement.

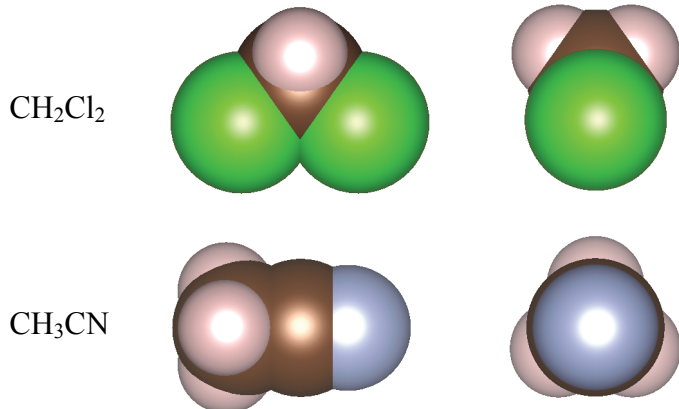


Fig. ESI-12. Molecular shape and size of CH_2Cl_2 (up) and CH_3CN (bottom). The molecules are illustrated with van der Waals radii. There is no large difference in shape and size between both molecules. This structural similarity might be a factor that TRI form sometimes appears in the case of CH_2Cl_2 .

References

- [1] H. Dan, S. Nishikiori and O. Yamamuro, *Dalton Trans.*, 2011, **40**, 1168.
- [2] P.-E. Werner, L. Eriksson and M. Westdahl, *J. Appl. Crystallogr.*, 1985, **18**, 367.
- [3] T. Kitazawa, S. Nishikiori, R. Kuroda and T. Iwamoto, *J. Chem. Soc., Dalton Trans.*, 1994, 1029.